catalysts

MDPI

Article

^{1}H NMR Analysis of the Metathesis Reaction between 1-Hexene and (*E*)-Anethole Using Grubbs 2nd Generation Catalyst: Effect of Reaction Conditions on (*E*)-1-(4-Methoxyphenyl)-1-hexene Formation and Decomposition

Marthinus Rudi Swart, Charlene Marais and Elizabeth Erasmus *

Department of Chemistry, University of the Free State, P.O. Box 339, Bloemfontein 9300, South Africa; SwartMR@ufs.ac.za (M.R.S.); MaraisC@ufs.ac.za (C.M.)
* Correspondence: ErasmusE@ufs.ac.za

Abstract: The metathesis of 1-hexene and (*E*)-anethole in the presence of Grubbs 2nd generation catalyst was monitored by in situ ^{1}H NMR spectroscopy at different temperatures (15 °C, 25 °C, and 45 °C) and anethole mol fractions ($X_{Anethole} \approx 0.17, 0.29, 0.5, 0.71, 0.83$). Time traces confirmed the instantaneous formation of (*E*)-1-(4-methoxyphenyl)-1-hexene, the cross-metathesis product. A maximum concentration of (*E*)-1-(4-methoxyphenyl)-1-hexene is reached fairly fast (the time depending on the reaction conditions), and this is followed by a decrease in the concentration of (*E*)-1-(4-methoxyphenyl)-1-hexene due to secondary metathesis. The maximum concentration of (*E*)-1-(4-methoxyphenyl)-1-hexene was more dependent on the $X_{Anethole}$ than the temperature. The highest TOF (3.46 min^{-1}) was obtained for the reaction where $X_{Anethole}$ was 0.16 at 45 °C. The highest concentration of the cross-metathesis product was however achieved after 6 min with an anethole mol fraction of 0.84 at 25 °C. A preliminary kinetic study indicated that the secondary metathesis reaction followed first order kinetics.

Keywords: Grubbs 2nd generation catalyst; reaction conditions; ^{1}H NMR analysis; cross-metathesis; self-metathesis; secondary metathesis

Citation: Swart, M.R.; Marais, C.; Erasmus, E. ^{1}H NMR Analysis of the Metathesis Reaction between 1-Hexene and (*E*)-Anethole Using Grubbs 2nd Generation Catalyst: Effect of Reaction Conditions on (*E*)-1-(4-Methoxyphenyl)-1-hexene Formation and Decomposition. *Catalysts* **2021**, *11*, 1483. https://doi.org/10.3390/catal11121483

Academic Editor: Bartosz Trzaskowski

Received: 22 October 2021
Accepted: 30 November 2021
Published: 3 December 2021

1. Introduction

Olefin metathesis is commonly used to convert alkenes into new alkenes with rearranged substituents through the intermediacy of a cyclometallacarbene [1–4]. The vast array of olefin metathesis applications includes, but are not limited to, cross-metathesis (CM), self-metathesis (SM), ene-yne metathesis, ring-opening metathesis (ROM), ring-closing metathesis (RCM) and ring-rearrangement metathesis (RRM) [3,4].

In recent years, the CM methodology to form carbon-carbon double bonds employing Grubbs catalysts have been investigated extensively and numerous review articles summarize this [2,4–11]. Cross-metathesis is a convenient synthetic approach to introduce a molecular fragment, often with a functional group, to a simple alkene to produce a value-added compound. Due to its functional group tolerance and stability, the imidazole-based Grubbs 2nd generation catalyst (see Figure 1 for the structure) is one of the most popular homogeneous olefin metathesis catalysts [1,3,6,12,13].

The formation of alkenes with asymmetric substitution through CM is however not inherently selective due to competing SM of the substrates [2,10,14,15]. Additionally, the desired asymmetric CM product, along with other CM and SM metathesis products, may participate in undesired secondary metathesis reactions [10,15–17]. The formation of regioisomers adds further complexity [18–20]. A study monitoring the formation and conversion of selected products in real time at different conditions is thus desirable to determine the ideal conditions for the formation of the target CM product in optimum yield.

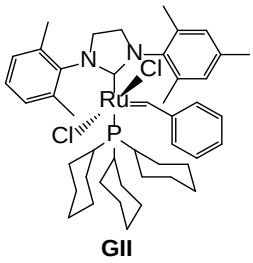

Figure 1. Structure of Grubbs 2nd generation catalyst, GII.

Alkenyl and alkyl arenes are important commodities and fine chemicals with applications in the production of plastics, elastomers, pharmaceuticals, detergents, flavours, fragrances, pheromones, etc. [21–23]. The traditional route to alkenyl and alkyl arenes via acid-catalyzed alkene arylation is hampered by polyalkylation and selectivity towards the branched product, amongst others [21,22].

In this study, hex-1-ene (1) and anethole (2) were selected as cross-metathesis partners due to the prevalence of anethole (2) and six-membered carbon chains in essential oils (renewable resource) [24–26]. Additional considerations included ease of handling (hex-1-ene (1) is a liquid) and the presence of well-resolved resonances to allow for monitoring by ^{1}H NMR spectroscopy.

The metathesis of 1-hexene (1) and (*E*)-anethole (2) by the Grubbs 2nd generation (GII) catalyst was thus studied with the objective to determine the effect of different reaction conditions on the rates of reagent consumption, self-metathesis, cross-metathesis and CM product consumption (stereoselectivity will not be considered during this investigation). A literature search in this regard did not return relevant publications pertaining to cross-metathesis. The consumption and formation rates were monitored in real time by ^{1}H NMR spectroscopy in $CDCl_3$ in a thermostatted NMR probe. Temperature (15 °C, 25 °C, and 45 °C) and substrate ratios (indicated as mole fraction, $X_{Anethole} \approx 0.83$, 0.71, 0.5, 0.29 and 0.17) were varied to determine the optimum reaction conditions and the ideal time to terminate the reaction to prevent secondary metathesis.

2. Results and Discussion

To determine if 1-hexene (1) and (*E*)-anethole (2) would be suitable substrates for the intended cross-metathesis reaction catalyzed by the Grubbs 2nd generation catalyst (see Figure 1 for the structure), ^{1}H NMR spectra of the starting materials and various metathesis products were acquired (Figure S12). ^{1}H NMR confirmed the alkene resonances of 1-hexene (1), as well as the methoxy and alkene resonances of (*E*)-anethole (2), to be easily distinguishable from each other and the resonances of (*E*)-1-(4-methoxyphenyl)-1-hexene (3), (*E*)-5-decene (5) and (*E*)-4,4′-dimethoxystilbene (7) (see Figures 2 and 3 for the reactions). Figure 3 shows various primary self- and cross-metathesis reaction pathways. Products of the CM2 pathway were however not observed by ^{1}H NMR and accordingly not discussed.

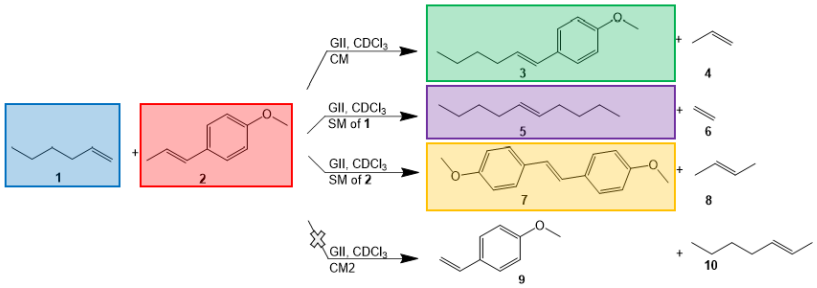

Figure 2. Primary cross-metathesis (CM) and self-metathesis (SM) reactions of 1-hexene (1) and (*E*)-anethole (2) to form (*E*)-1-(4-methoxyphenyl)-1-hexene (3), propene (4), (*E*)-5-decene (5), ethene (6), (*E*)-4,4′-dimethoxystilbene (7), (*E*)-2-butene (8), 4-methoxystyrene (9), and (*E*)-2-heptene (10).

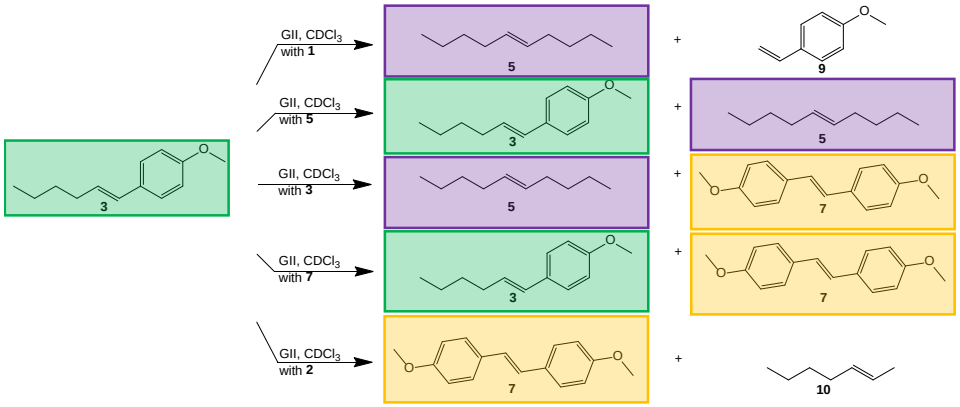

Figure 3. Secondary metathesis reactions of (*E*)-1-(4-methoxyphenyl)-1-hexene (3) with the original substrates and primary metathesis products to form (*E*)-5-decene (5), (*E*)-4,4′-dimethoxystilbene (7), 4-methoxystyrene (9), and (*E*)-2-heptene (10).

Starting with 1 and 2 in equivalent amounts ($X_{Anethole} = \frac{n_{anethole}}{n_{anethole}+n_{hex-1-ene}} \approx 0.5$) and GII (5 mol%) in $CDCl_3$ at 25 °C, the rate of substrate consumption (1 and 2), the rates of CM product (3) and SM product (5 and 7) formation, as well as the rates of secondary metathesis reactions were monitored. Figure 4 shows the ^1H NMR spectral regions used for the real time monitoring of substrate and product concentrations at different time intervals for experiment 4 as an example. The isomerization [27–30] of hex-1-ene (1), 5-decene (5) and heptene (10) and the participation of these isomers, together with other metathesis by-products such as ethene (6), propene (4) and butene (8) in metathesis reactions, cannot be excluded. Certain resonances may thus be ascribed to the expected compounds and homologues thereof: the ddt corresponding to H-2 of hex-1-ene (1) may therefore also be ascribed to other terminal alkenes; the dd corresponding to H-1 of (*E*)-1-(4-methoxyphenyl)-1-hexene (3) may include H-1 of homologues with four or more carbons in the side chain, and the multiplet corresponding to H-5 of 5-decene (5) may include other internal alkene resonances [31,32]. The time trace of experiment 4, prepared from the data obtained in Figure 4, appear in Figure 5. The time dependent ^1H NMR spectra of experiments 1–11 (see Table 1 for the reaction conditions) are presented in the Supplementary Information (Figures S1–S12), whereas the time traces for reactions 1–11 can be found in the Supplementary Information, Figure S13.

During the early stages of experiment 4, the conversion of 1-hexene (1) occurs almost twice as fast as that of (*E*)-anethole (2) (see Figure 5A). This correlates with the metathesis selectivity model according to which internal olefins (such as 2 and 5) are less reactive than terminal olefins (such as 1) [17,29,33]. The simultaneous formation of the desired CM product 3 (green line) and the undesired SM products 5 (SM of 1, purple line) and 7 (SM of 2, yellow line), are observed from the onset of the reaction with the rate of formation decreasing in the order 5 > 3 > 7. The maximum concentration (0.051 M) of the CM product (3) was reached after 12 min, with the concentration of 5 being more than five times that of 7 (0.084 M and 0.016 M respectively) at this time. At 12 min, 66% of the 1-hexene (1) had been consumed in comparison to only 36% of the (*E*)-anethole (2). Nelson et al. similary reported the cross-metathesis product of 3-phenylprop-1-ene and (*Z*)-1,4-diacetoxy-2-butene to be formed in optimum concentration after only 17 min [GII (2.5 mol%), 25 °C] [34].

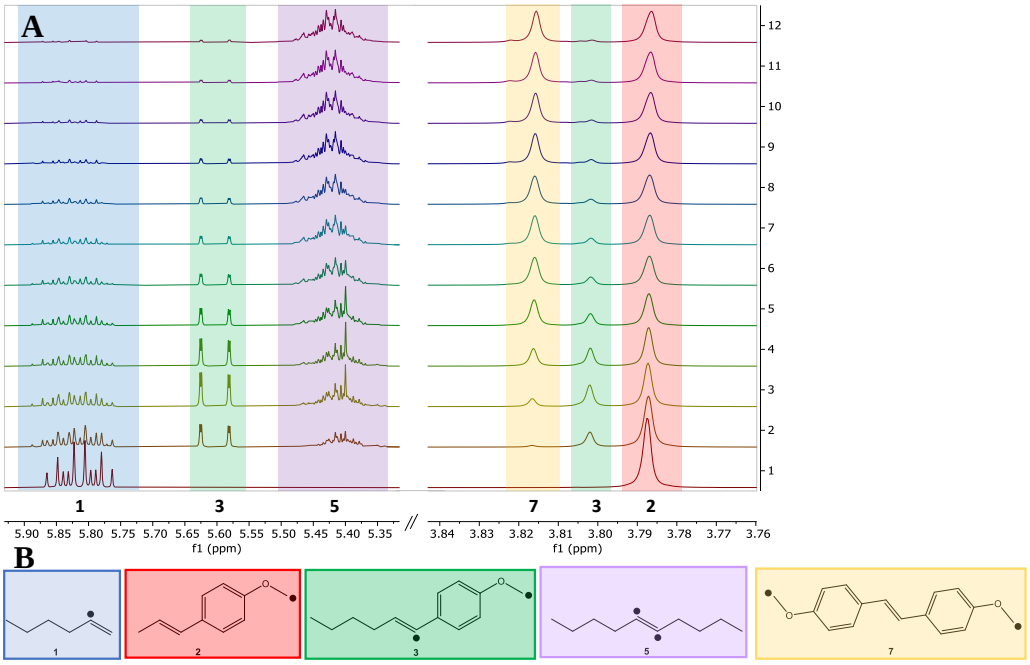

Figure 4. (**A**) The time dependent ^{1}H NMR spectra of the crude metathesis reaction mixture between (*E*)-anethole and 1-hexene ($X_{Anethole} \approx 0.5$) in the presence of Grubbs 2nd generation catalyst at 25 °C in $CDCl_3$ (experiment 4). The spectra at times t = 0 min. (1), t = 4 min. (2), t = 16 min. (3), t = 49 min. (4), t = 102 min. (5), t = 175 min. (6), t = 268 min. (7), t = 371 min. (8), t = 504 min. (9), t = 657 min. (10), t = 830 min. (11) and t = 1023 min. (12) are shown. The designated resonances belonging to 1 is indicated in the blue box, 2 red, 3 green, 5 purple, and 7 yellow. (**B**) (•) indicates the designated hydrogen ^{1}H NMR resonances used as characteristic compound identifiers.

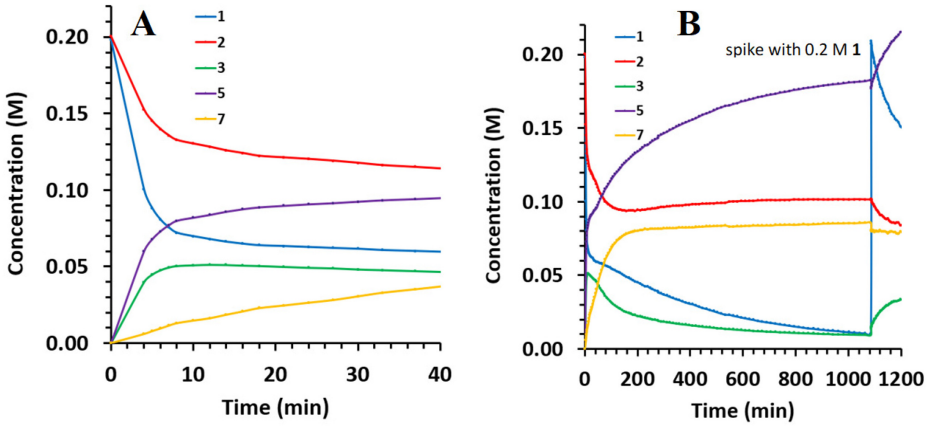

Figure 5. The time trace (of experiment 4) of the Grubbs 2nd generation catalysed (*E*)-anethole and 1-hexene ($X_{Anethole} \approx 0.5$) reaction at 25 °C in $CDCl_3$ (**A**) 0–40 min, and (**B**) 0–1200 min (with a spike of 1-hexene at 1086 min) of the integrated values of the disappearance of the starting materials, (*E*)-anethole (2, red -) and 1-hexene (1, blue -), and the formation of the different products, CM (3, green -), SM 1-hexene (5, purple -) and SM (*E*)-anethole (7, yellow -).

Table 1. Table depicting moles of reagents, mole ratios of reagents, mole fraction (X) of (*E*)-anethole, and temperatures of reactions.

Exp No	Temp (°C)	Mole Substrate		Substrate Concentration		$X_{Anethole}$	Mole Ratio	Spike after 18 h	
		1-hexene (mmol)	(*E*)-anethole (mmol)	1-hexene (M)	(*E*)-anethole (M)		1-hexene:(*E*)-anethole	1-hexene (mmol)	(*E*)-anethole (mmol)
1	15	0.119	0.114	0.20	0.19	0.49	1.00:0.96		
2		0.594	0.117	0.99	0.20	0.16	5.08:1.00		
3		0.295	0.12	0.49	0.20	0.29	2.46:1.00		
4	Exp No 2	0.118	0.12	0.20	0.20	0.5	1.00:1.02		
5		0.118	0.325	0.20	0.54	0.73	1.00:2.75		
6		0.118	0.599	0.20	1.00	0.84	1.00:5.08		
7		0.594	0.114	0.99	0.19	0.16	5.21:1.00		
8		0.297	0.112	0.50	0.19	0.27	2.65:1.00		
9	Exp No 7	0.118	0.115	0.20	0.19	0.49	1.00:0.97		
10		0.119	0.299	0.20	0.50	0.72	1.00:2.51		
11		0.119	0.592	0.20	0.99	0.83	1.00:4.97		
12		0.118	0.12	0.20	0.20	0.5	1.00:1.02	0.119	
13	Exp No 12	0.119	0.113	0.20	0.19	0.49	1.00:0.95		0.113
14		0.119	0.113	0.20	0.19	0.49	1.00:0.95	0.117	0.113

During the next stage of the reaction (from ca. 12 min to ca. 45 min), the concentration of 3 starts to decrease due to secondary metathesis, while the concentrations of both 5 and 7 continue to increase (see Figure 5B).

From ca. 45 min onwards, the last stage of the reaction, the decrease in concentration of 3 is accompanied by an increase in the concentration of 5. The formation of 7, on the contrary, increases to a steady state at ca. 0.084 M and 7 seems to be in equilibrium with 2, which reaches a steady state at ca. 0.10 M, i.e. half the initial concentration thereof (see Figure 5B).

After 18 h, the reaction was spiked with 0.2 M of 1 (experiment 12, see Figure 5B for the time trace). This resulted in the formation of additional 3 and 5 and consumption of 1 and 2, indicating that the catalyst was still active. Spiking the reaction mixture with 2 (experiment 13), or with a both 1 and 2 (experiment 14), also resulted in an increase in 3, but not in such a drastic manner as with only 1 (see Figure S14 in the Supplementary Information). Unlike the initial step of the reaction where the CM product (3) reached a maximum concentration after ca. 12 min. and then decreased, spiking resulted in an increase in the concentration of 3, which then reached and maintained a steady state (and no decrease in the concentration).

A comparative investigation of the initial stages of the reactions under different reaction conditions was conducted (experiments 1–11, see Table 1), focussing on the first 20 min of the reaction. The time traces of these experiments are represented in Figure 6 (all time traces for reactions 1–11 are presented in the Supplementary Information, Figure S13).

Firstly, as expected, an increase in temperature (T = 15 °C, 25 °C, and 45 °C) whilst keeping the substrate concentration at a 1:1 ratio (1-hexene:(*E*)-anethole, $X_{Anethole} \approx 0.5$), resulted in an increase in the consumption of 1 and 2 along with the appearance of 5 and 7 (for clarity, the enlarged graphs are shown in Figure S15 in the Supplementary Information). This correlates well with independent results reported by Carrasco et al. [27] and Nelson et al. [34], who reported the initiation rate constant (k_{int}) of GII to be ca. $x10^3$ higher ($k_{int} = 1.3 \times 10^{-1}$) at 80 °C than at 40 °C ($k_{int} = 1.8 \times 10^{-4}$).

The experiments at both 15 °C and 25 °C (experiments 1 and 4, respectively) showed a reagent consumption of ca. 1:0.5 (1-hexene:(*E*)-anethole) after the first 4 min. At 45 °C, 0.6 mole of (*E*)-anethole was consumed for every 1 mole of 1-hexene after 4 min, with a total consumption of 70% of 1 in 4 min (experiment 9). CM product (3) formation (see Figure 7 A for the time traces of CM at different temperatures with $X_{Anethole} \approx 0.5$) was the fastest during the first 4 min at all three temperatures. At the lower temperature (15 °C), the concentration of 3 continued to increase slowly to a maximum of 0.046 M at 102 min (Figure S12). An advantage of conducting a reaction at this low temperature is that the

secondary metathesis reaction is also greatly suppressed and the secondary metathesis of the desired CM product, 3, is thus also slow.

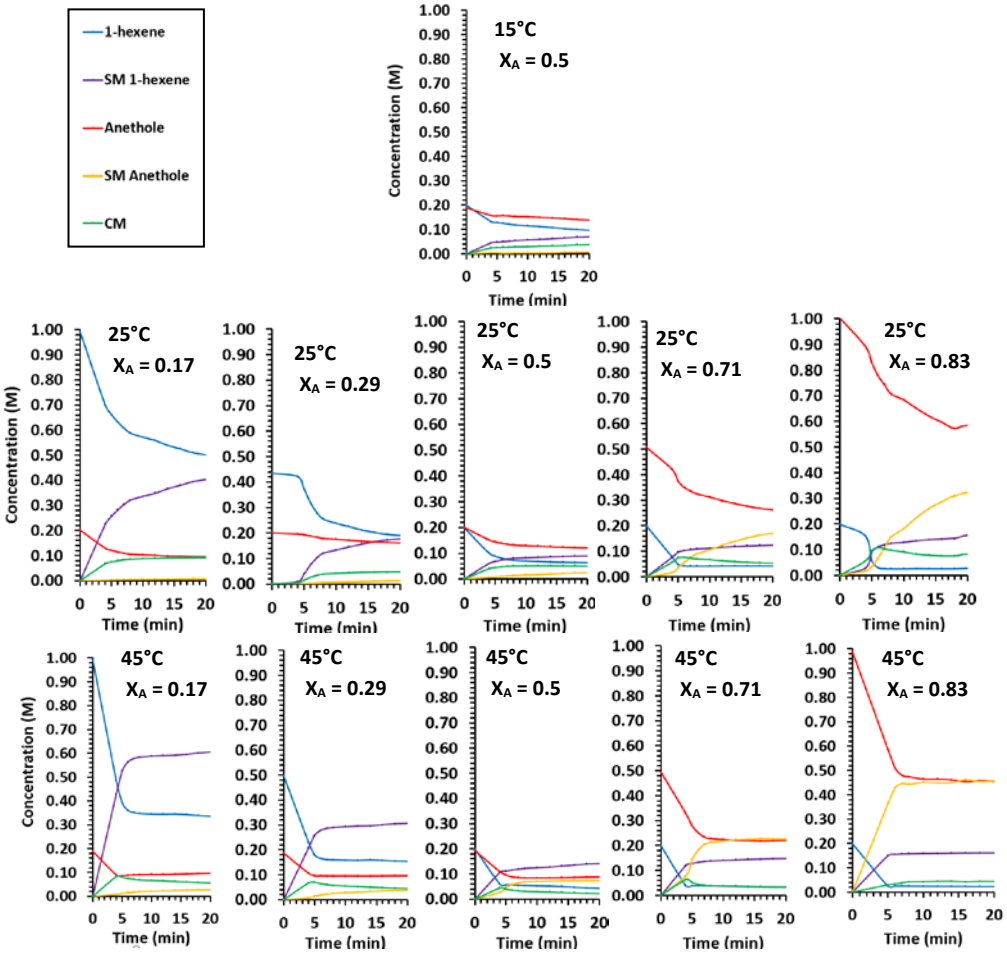

Figure 6. The time traces of the initial 20 min of the Grubbs 2nd generation catalysed metathesis reaction between 1-hexene (1) and (*E*)-anethole (2) at 15 °C (top row), 25 °C (middle row), and 45 °C (bottom row), the mole fraction of (*E*)-anethole is indicated on each graph.

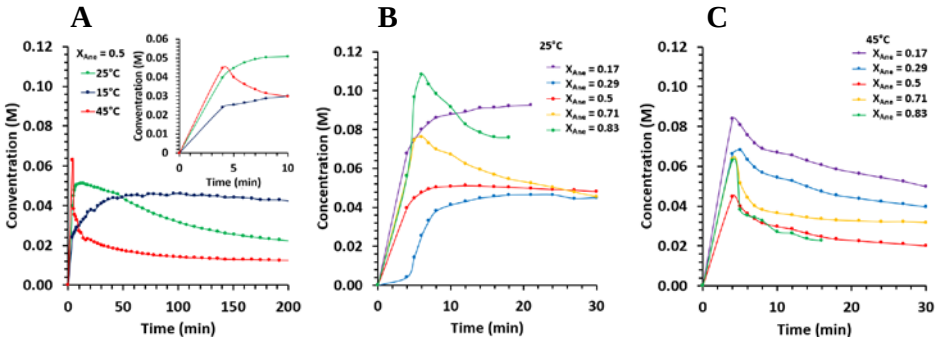

Figure 7. The time traces of the formation of the CM product **3** during the Grubbs 2nd generation catalysed metathesis reaction between 1-hexene (**1**) and (*E*)-anethole (**2**) at (**A**) 15 °C (blue line), 25 °C (green line), and 45 °C (red line) with $X_{Anethole} \approx 0.5$, (**B**) 25 °C with $X_{Anethole} \approx 0.83$ (green line), $X_{Anethole} \approx 0.71$ (yellow line), $X_{Anethole} \approx 0.5$ (red line), $X_{Anethole} \approx 0.29$ (blue line), and $X_{Anethole} \approx 0.17$ (purple line), as well as (**C**) 45 °C with $X_{Anethole} \approx 0.83$ (green line), $X_{Anethole} \approx 0.71$ (yellow line), $X_{Anethole} \approx 0.5$ (red line), $X_{Anethole} \approx 0.29$ (blue line), and $X_{Anethole} \approx 0.17$ (purple line).

It is important to note that at 45 °C, which falls in the range commonly used in metathesis reactions [6,28,29], the maximum recorded concentration of 3 (0.046 M) was measured at ca. 4 min, i.e. the minimum acquisition time possible for the instrument. Based on the reagent consumption ratio, the true maximum concentration may have been reached earlier, though. Nevertheless, the concentration of 3 decreases rapidly after 4 min at 45 °C (see Figure 7A, red line). This implies that, despite fast formation kinetics of 3, secondary metathesis sets in at a more rapid pace in comparison to reactions at lower temperatures. Van der Gryp et al. also found secondary metathesis to increase dramatically with an increase in temperature [30].

At 25 °C, the rate to reach the maximum concentration of 3 under these experimental conditions ($X_{Anethole}$ = 0.5), is slightly slower than at 45 °C. The maximum concentration of 3 is slightly higher ($[3]_{max}$ = 0.051 M) at 25 °C in comparison to 45 °C ($[3]_{max}$ = 0.046 M), though, and was reached in 12 min (vs 4 min at 45 °C). Concurrently, the secondary metathesis reaction and subsequent CM product loss is also slower at the lower temperature. At 25 °C, cross-metathesis was thus achieved within a reasonable time, but still slow enough for the reaction to be monitored and terminated timeously to obtain $[3]_{max}$.

Keeping the temperature constant, the next reaction condition under investigation was the mole ratios of the two reagents, 1-hexene (1) and (*E*)-anethole (2), (see Figure 7B,C for the time traces at 25 °C and 45 °C for the formation of 3 at different $X_{Anethole}$). Due to the slow kinetics at 15 °C, additional experiments at this temperature were not conducted (since it is too time consuming and thus not economically viable).

At 25 °C, 3 was obtained the fastest and in the highest concentration with one of the reagents in five fold excess (experiments 2 and 6). As indicated in Figure 7B, experiment 6, an anethole mol fraction of ≈ 0.83 ((*E*)-anethole, 2, in five fold excess) gave 3 in the highest concentration (0.108 M) after only 6 min. However, secondary metathesis under these reaction conditions sets in quickly over the next 15 min. 1-Hexene (1) in a factor five excess ($X_{Anethole}$ ≈ 0.17) resulted in a slightly lower maximum concentration of 3 (0.092 M) after a longer period (21 min). The rate of secondary metathesis for experiment 2 is, however, also much slower. Where $X_{Anethole}$ ≈ 0.83 (experiment 6), the concentration of 1-hexene (1) seem to reach a steady-state after 6 min (see Figure S13), though the concentrations of (*E*)-anethole (2) and CM product 3 continue to decrease while the (*E*)-4,4′-dimethoxystilbene (7) concentration increases, thus indicating the continuation of both self-metathesis of 2 and secondary metathesis between 3 and 2. The concentration of (*E*)-5-decene (5), the SM of 1, continues to increase despite the concentration of **1** being constant, thus confirming secondary metathesis of 3 to form 5 and 7. When the less reactive (*E*)-anethole (2) is the limiting reagent [$X_{Anethole}$ ≈ 0.17 (experiment 2)], it reacts readily to ca. half the initial concentration (within the first 8 min), whereafter the concentration slowly increases over time.

Figure 7C shows similar time traces for the formation of 3 at 45 °C at different $X_{Anethole}$. The reactions all peaked at ca. four minutes, with $X_{Anethole}$ = 0.16 giving the highest concentration of 3 (0.083 M) and $X_{Anethole}$ = 0.83 the third highest (0.062 M). At 45 °C, the onset and rate of secondary metathesis are fast for all the reactions (Figure S13).

Following the initial fast consumption of 2, a slight increase in the concentration of (*E*)-anethole (2) is observed (see Figure S13). At 45 °C with $X_{Anethole}$ = 0.16, 0.27 and 0.49, and at 25 °C with $X_{Anethole}$ = 0.16 and 0.73, the concentration of (*E*)-anethole (2) reaches a minimum after 4, 5, 10, 27, and 58 min, respectively, followed by a slight increase in concentration. This coincides with a decrease in the concentration of cross-metathesis product 3 and can thus be ascribed to secondary metathesis of the latter. No secondary metathesis of stilbene 7 was observed under any of the conditions investigated.

A summary of the maximum concentrations observed for 3 ($[3]_{max}$) and the time to reach $[3]_{max}$ under different conditions, is presented in Table 2 and Figure 8. From Figure 8A, the highest maximum concentration of 3 (0.108 M) was obtained at 25 °C with $X_{Anethole}$ = 0.84 (experiment 6), followed by 0.092 M at 25 °C and $X_{Anethole}$ = 0.16 (experiment 2), both higher than $[3]_{max}$ observed at 45 °C (0.083 M, $X_{Anethole}$ = 0.16, experiment 7)

(It must be granted, though, that inherent instrument restrictions only allowed for analysis after 4 min and that the peak concentration may have been reached earlier at 45 °C). An excess of one of the reagents is therefore required to obtain the highest possible concentration of the cross-metathesis product (3). Additionally, a moderate temperature of 25 °C afforded higher yields of the CM product 3. Regarding the time required to reach the respective maximum concentrations (see Figure 8B), higher temperatures gave $[3]_{max}$ faster, with 25 °C reactions being more manageable and those at 15 °C being very slow. At 25 °C, the time to reach $[3]_{max}$ decreases as the $X_{Anethole}$ increases. Taking all the variations into consideration, the optimum conditions for the cross-metathesis of 1-hexene (1) and (*E*)-anethole (2) in the presence of the Grubbs 2nd generation catalyst are 25 °C, at least a five fold excess of (*E*)-anethole and termination of the reaction after 6 min. A five fold excess of 1-hexene (which is the more economical reagent), however, also results in a comparative yield of 3. This reaction can proceed for 20 min before secondary metathesis sets in.

Table 2. Summary of the experiment number, $X_{Anethole}$, temperature, time to reach the maximum concentration of 3, the maximum concentration of 3 and the turnover frequency (TOF) until $[3]_{max}$ is achieved. The relative percentages of metathesis products 3, 5, and 7 at the time when $[3]_{max}$ was reached, is summarized.

Exp No	$X_{Anethole}$	Temp (°C)	Maximum [3]		TOF t $[3]_{max}$ (min^{-1})	k'_{obs} 3 Disappearance (min^{-1})	% Distribution at the Time When $[3]_{max}$ Was Reached		
			Time (min)	[3] (M)			3	5	7
1	0.49	15	102	0.046	0.08	0.0008	28.9	59.4	11.7
2	0.16	25	21	0.092	0.64	0.0042	18.2	80.3	1.6
3	0.29	25	18	0.046	0.43	0.0128	19.8	74.7	5.5
4	0.50	25	12	0.051	0.71	0.0064	33.8	55.5	10.7
5	0.73	25	6	0.076	2.11	0.0218	32.2	43.6	24.1
6	0.84	25	6	0.108	3.00	0.0352	37.9	38.6	23.5
7	0.16	45	4	0.083	3.46	0.0515	15.9	82.5	1.6
8	0.27	45	5	0.068	2.27	0.0447	20.0	75.9	4.1
9	0.49	45	4	0.045	1.88	0.0681	25.2	59.5	15.3
10	0.72	45	4	0.064	2.67	0.1278	24.3	45.4	30.3
11	0.83	45	4	0.069	2.88	0.2892	14.9	32.9	52.2

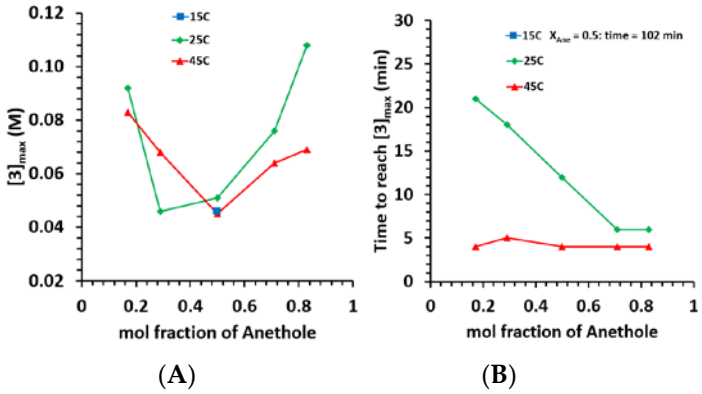

(**A**) (**B**)

Figure 8. (**A**) Graph comparing $[3]_{max}$ against $X_{Anethole}$ at the different temperatures (15 °C blue, 25 °C green line, 45 °C red line). (**B**) Graph comparing the time to reach $[3]_{max}$ against $X_{Anethole}$ at the different temperature (15 °C blue, 25 °C green line, 45 °C red line).

Theoretically, the statistical distribution of the metathesis products formed between olefins with similar reactivity (assuming full conversion and no secondary metathesis) is 50% for the CM product and 25% each for the two SM products [35]. In the current study, the relative percentages of the metathesis products 3:5:7 at the time when $[3]_{max}$ was

reached (see Table 2 and Figure S16), deviated from the 50%:25%:25% distribution, with a ratio of 33.8%:55.5%:10.7% being observed in experiment 4, for example, and self-metathesis product 5 being present in larger quantities (apart from experiment 11). Another interesting observation was that the relative percentages of the products are more dependent on $X_{Anethole}$ than the temperature (at the time where $[3]_{max}$ is reached) as the percentages are comparable at different temperatures and at the same $X_{Anethole}$ (Figures S16 and S17).

The rate of secondary metathesis of 3, after $[3]_{max}$ was reached, could also be determined. The disappearance of 3 followed first order kinetics and accordingly the apparent observed first order rate constant (k'_{obs}) for the secondary metathesis of 3 was determined for all the experiments (see Table 2). The kinetic plots used to determine the k'_{obs} are shown in Figure 9A–C. Comparing the rate of secondary metathesis of 3 (Figure 9D), indicated that, as expected, a higher temperature resulted in the faster disappearance of 3. Additionally, as the $X_{Anethole}$ increased, a drastic increase in secondary metathesis was also observed (at both 25 °C and 45 °C). This implies that the presence of excess (*E*)-anethole (2) is a driving force for secondary metathesis. Thus, it is more desirable to use 1 in excess since it results in slower secondary metathesis.

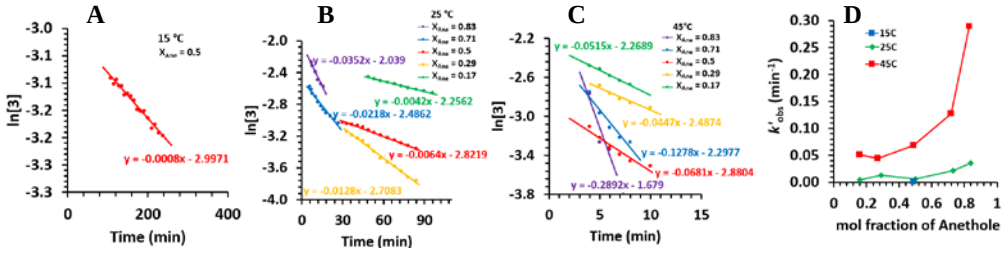

Figure 9. The kinetic plots of the disappearance of 3 at (**A**) 15 °C, (**B**) 25 °C and (**C**) 45 °C for the secondary metathesis reactions (at the indicated $X_{Anethole}$) that leads to the apparent observed first order rate constant k'_{obs} for the secondary metathesis of 3. (**D**) Graph comparing the k'_{obs} for the secondary metathesis of 3 at 15 °C (blue), 25 °C (green) and 45 °C (red) against the $X_{Anethole}$.

Most kinetic studies reported for metathesis reactions catalysed by Grubbs' catalysts focus on the mechanistic pathways of the catalyst itself [36–40]. From the data reported in this study, the optimal reaction conditions to achieve the highest catalyst turnover frequency (TOF), were determined. The TOF was calculated at the time when $[3]_{max}$ was reached, see Table 2, and was determined using Equation (1):

$$\text{TOF} = \frac{\left(\frac{\text{mol } [3]_{max}}{\text{mol catalyst}}\right)}{\text{time to reach } [3]_{max}} \quad (1)$$

Though the optimal reaction conditions for the highest $[3]_{max}$ were 25 °C with the $X_{Anethole}$ = 0.84 and $t_{terminate}$ = 6 min (experiment 6), the highest TOF was obtained at 45 °C with $X_{Anethole}$ = 0.16 and $t_{terminate}$ = 4 min (experiment 7, 3.46 min^{-1}). Our results are in correlation with both Dinger et al. and van der Gryp et al., who reported the highest turnover numbers (TON) for the Grubbs and Hoveyda-Grubbs 2nd generation catalysts at temperatures between 50 °C and 80 °C [30,41]. This confirms that the conditions to achieve optimal catalyst performance are not necessarily those that give the highest yield of the CM product (3). Optimal reaction conditions, as determined previously, did however result in the second highest TOF (3.00 min^{-1}), whereas the most practical and economical reaction conditions (experiment 2, $X_{Anethole}$ = 0.16, 25 °C) only resulted in a TOF of 0.64 min^{-1}.

3. Materials and Methods

3.1. General

The Grubbs 2nd generation catalyst [1,3-bis(2,4,6-trimethylphenyl)-2-imidazolidinylidene)dichloro(phenylmethylene)(tricyclohexylphosphino)ruthenium], (*E*)-anethole (99%),

1-hexene (97%) and solvents used in this study were purchased from Sigma-Aldrich (Sigma-Aldrich Pty. Ltd., Johannesburg, South-Africa) and were used under inert conditions without further purification. Solvents were dried through a small column of activated neutral alumina (10% *v*/*v*) prior to use.

3.2. Spectroscopic Characterisation Techniques

3.2.1. ^{1}H NMR Spectroscopy

^{1}H NMR spectra were recorded at various temperatures on either a Bruker 400 MHz AVANCE III NMR spectrometer (Bruker, Rheinstetten, Germany) or a Bruker 600 MHz AVANCE II NMR spectrometer (Bruker, Rheinstetten, Germany) operating at 400.16 MHz and 600.28 MHz, respectively, for the ^{1}H frequency. Reported hydrogen shifts are relative to tetramethylsilane (TMS) in $CDCl_3$ at δ0.00 ppm.

3.2.2. Monitoring of the Metathesis Reactions

The metathesis reactions between 1-hexene and (*E*)-anethole, catalysed by Grubbs 2nd generation catalyst, were monitored in situ by ^{1}H NMR spectroscopy (in $CDCl_3$) in a thermostatted NMR probe.

1-Hexene (see Table 1 for mmol, M and mole fraction) and (*E*)-anethole (see Table 1 for mmol, M and mole ratio) were dissolved in $CDCl_3$ (0.6 mL) with Grubbs 2nd generation catalyst (0.006 mmol; 5 mol %), transferred to a standard Aldrich NMR tube under an argon atmosphere and the tube closed with a standard end cap. ^{1}H NMR spectra were recorded at various time intervals for ca. 18 h at 15 °C, 25 °C and 45 °C. The reaction for the $X_{Anethole}$ = 0.83 (1:5 ratio for 1-hexene:(*E*)-anethole) was followed up to the point where precipitation of (*E*)-4,4′-dimethoxystilbene (7) impaired NMR measurements (ca.18 min). The concentration of each reagent and product was determined in M by integration of characteristic resonances with TMS as an internal standard ($\int$ 1.0). Since the initial concentrations of the 1-hexene and (*E*)-anethole are known, and the concentration of TMS does not change over time, using the ratio between the integral of the TMS and characteristic resonances of the starting materials and products, the concentrations of starting materials and products [C_x] at various times (t) could be calculated by using Equation (2):

$$[C_x]_t = \frac{(I_x)_t \times [C]_0}{(I)_{tot}} \quad (2)$$

$[C_x]_t$ = Concentration of compound (*x*) at time t
$[C]_0$ = Concentration of reagents at time 0
$(I_x)_t$ = Sum of resonance integrals ($\int$) for compound (x) at time t
$(I)_{tot}$ = Total resonance integrals ($\int$) of reaction mixture at time t

4. Conclusions

In the metathesis reaction of 1-hexene (1) and (*E*)-anethole (2) catalyzed by Grubbs 2nd generation catalyst, more 1-hexene (1) is consumed as a percentage of the initial concentration compared to (*E*)-anethole, irrespective of the $X_{Anethole}$. This may be attributed to the terminal olefin, 1-hexene (1), being more active than the internal olefin, (*E*)-anethole (2).

Spiking the reaction (where $X_{Anethole} \approx 0.5$ at 25°C) with either one or both of the substrates, resulted in further metathesis reactions, thus confirming that the catalyst was still active after 18 h reaction time. Spiking the reaction mixture with 1-hexene (1) resulted in the best metathesis outcome with (*E*)-1-(4-methoxyphenyl)-1-hexene (3) forming once again and no indication of secondary metathesis (even after 240 min).

In line with Le Chateliers principle, the highest possible concentration for the cross-metathesis reactions was obtained when one of the reagents was present in five-fold excess. The highest maximum concentration of 3 ($[3]_{max}$ = 0.108 M) was obtained at 25 °C with $X_{Anethole}$ = 0.84 after 6 min, followed by 25 °C and $X_{Anethole}$ = 0.16 resulting in $[3]_{max}$ = 0.092 M. With $X_{Anethole}$ = 0.16 at 25 °C giving a good cross-metathesis yield,

1-hexene (1) being the cheaper reagent and the absence of secondary metathesis during the first 20 min, these were selected as the preferred conditions.

The secondary metathesis of 3 followed first order kinetics under all the reaction conditions investigated. A comparison of the k'_{obs} values indicated that an increase in the $X_{Anethole}$ resulted in an increase in secondary metathesis (at both 25 °C and 45 °C). It can thus be concluded that the presence of an excess (*E*)-anethole (2) is a driving force for secondary metathesis. This furthermore confirms that the use of 1-hexene (1) (the terminal olefin) as the reagent in excess is more desirable since it results in slower secondary metathesis, is more affordable, gives a high $[3]_{max}$ and also results in reactions slow enough to be monitored for timeous termination.

Supplementary Materials: The following are available online at https://www.mdpi.com/article/10.3390/catal11121483/s1, Figure S1: The time dependent ^{1}H NMR spectra of crude metathesis reaction mixture between (*E*)-anethole and 1-hexene ($X_{Anethole}$ = 0.5) in the presence of Grubbs 2nd generation catalyst at 15 °C in $CDCl_3$ (experiment 1). The spectra at times t = 0 min. (1), t = 4 min. (2), t = 16 min. (3), t = 49 min. (4), t = 102 min. (5), t = 175 min. (6), t = 268 min. (7), t = 371 min. (8), t = 504 min. (9), t = 657 min. (10) and t = 724 min. (11), Figure S2: The time dependent ^{1}H NMR spectra of crude metathesis reaction mixture between (*E*)-anethole and 1-hexene ($X_{Anethole}$ = 0.17) in the presence of Grubbs 2nd generation catalyst at 25 °C in $CDCl_3$ (experiment 2). The spectra at times t = 0 min. (1), t = 4 min. (2), t = 16 min. (3), t = 49 min. (4), t = 102 min. (5), t = 175 min. (6), t = 268 min. (7), t = 371 min. (8), t = 504 min. (9), t = 657 min. (10), t = 830 min. (11) and t = 1023 min. (12), Figure S3: The time dependent ^{1}H NMR spectra of crude metathesis reaction mixture between (*E*)-anethole and 1-hexene ($X_{Anethole}$ = 0.23) in the presence of Grubbs 2nd generation catalyst at 25 °C in $CDCl_3$ (experiment 3). The spectra at times t = 0 min. (1), t = 4 min. (2), t = 16 min. (3), t = 49 min. (4), t = 102 min. (5), t = 175 min. (6), t = 268 min. (7), t = 371 min. (8), t = 504 min. (9) and t = 657 min. (10), Figure S4: The time dependent ^{1}H NMR spectra of crude metathesis reaction mixture between (*E*)-anethole and 1-hexene ($X_{Anethole}$ = 0.5) in the presence of Grubbs 2nd generation catalyst at 25 °C in $CDCl_3$ (experiment 4). The spectra at times t = 0 min. (1), t = 4 min. (2), t = 16 min. (3), t = 49 min. (4), t = 102 min. (5), t = 175 min. (6), t = 268 min. (7), t = 371 min. (8), t = 504 min. (9), t = 657 min. (10), t = 830 min. (11) and t = 1023 min. (12). Figure S5: The time dependent ^{1}H NMR spectra of crude metathesis reaction mixture between (*E*)-anethole and 1-hexene ($X_{Anethole}$ = 0.71) in the presence of Grubbs 2nd generation catalyst at 25 °C in $CDCl_3$ (experiment 5). The spectra at times t = 0 min. (1), t = 4 min. (2), t = 16 min. (3), t = 49 min. (4), t = 102 min. (5), t = 175 min. (6), t = 268 min. (7), t = 371 min. (8), t = 504 min. (9) and t = 657 min. (10), Figure S6: The time dependent ^{1}H NMR spectra of crude metathesis reaction mixture between (*E*)-anethole and 1-hexene ($X_{Anethole}$ = 0.83) in the presence of Grubbs 2nd generation catalyst at 25 °C in $CDCl_3$ (experiment 6). The spectra at times t = 0 min. (1), t = 5 min. (2), t = 8 min. (3), t = 14 min. (4), t = 21 min. (5), Figure S7: The time dependent ^{1}H NMR spectra of crude metathesis reaction mixture between (*E*)-anethole and 1-hexene ($X_{Anethole}$ = 0.17) in the presence of Grubbs 2nd generation catalyst at 45 °C in $CDCl_3$ (experiment 7). The spectra at times t = 0 min. (1), t = 4 min. (2), t = 7 min. (3), t = 16 min. (4), t = 30 min. (5), t = 49 min. (6), t = 73 min. (7), t = 102 min. (8), t = 136 min. (9), t = 175 min. (10) and t = 210 min. (11), Figure S8: The time dependent ^{1}H NMR spectra of crude metathesis reaction mixture between (*E*)-anethole and 1-hexene ($X_{Anethole}$ = 0.23) in the presence of Grubbs 2nd generation catalyst at 45 °C in $CDCl_3$ (experiment 8). The spectra at times t = 0 min. (1), t = 4 min. (2), t = 7 min. (3), t = 16 min. (4), t = 30 min. (5), t = 49 min. (6), t = 73 min. (7), t = 102 min. (8), t = 136 min. (9), t = 175 min. (10) and t = 219 min. (11), Figure S9: The time dependent ^{1}H NMR spectra of crude metathesis reaction mixture between (*E*)-anethole and 1-hexene ($X_{Anethole}$ = 0.5) in the presence of Grubbs 2nd generation catalyst at 45 °C in $CDCl_3$ (experiment 9). The spectra at times t = 0 min. (1), t = 4 min. (2), t = 7 min. (3), t = 16 min. (4), t = 30 min. (5), t = 49 min. (6), t = 73 min. (7), t = 102 min. (8), t = 136 min. (9), t = 175 min. (10) and t = 228 min. (11), Figure S10: The time dependent ^{1}H NMR spectra of crude metathesis reaction mixture between (*E*)-anethole and 1-hexene ($X_{Anethole}$ = 0.71) in the presence of Grubbs 2nd generation catalyst at 45 °C in $CDCl_3$ (experiment 10). The spectra at times t = 0 min. (1), t = 4 min. (2), t = 7 min. (3), t = 16 min. (4), t = 30 min. (5), t = 49 min. (6), t = 73 min. (7), t = 102 min. (8), t = 136 min. (9) and t = 192 min. (10), Figure S11: The time dependent ^{1}H NMR spectra of crude metathesis reaction mixture between (*E*)-anethole and 1-hexene ($X_{Anethole}$ = 0.83) in the presence of Grubbs 2nd generation catalyst at 45 °C in $CDCl_3$ (experiment 11). The

spectra at times t = 0 min. (1), t = 4 min. (2), t = 7 min. (3), t = 16 min. (4), t = 30 min. (5), t = 49 min. (6), t = 73 min. (7), t = 102 min. (8), t = 136 min. (9), t = 175 min. (10) and t = 201 min. (11), Figure S12: Expanded ^{1}H NMR spectra of reagents (1) 1-hexene (1); (2) (*E*)-anethole (2); (3) SM product of (2), (E)-4,4′-dimethoxystilbene (7); (4) SM product of (1), (E)-5-decene (5); and the crude metathesis reaction mixture between (*E*)-anethole and 1-hexene in the presence of Grubbs 2nd generation at t = 10 min. in $CDCl_3$ for (5) $X_{Anethole}$ = 0.5 at 15 °C; (6) $X_{Anethole}$ = 0.17 at 25 °C; (7) $X_{Anethole}$ = 0.29 at 25 °C; (8) $X_{Anethole}$ = 0.5 at 25 °C; (9) $X_{Anethole}$ = 0.71 at 25 °C; (10) $X_{Anethole}$ = 0.83 at 25 °C; (11) $X_{Anethole}$ = 0.17 at 45 °C; (12) $X_{Anethole}$ = 0.29 at 45 °C; (13) $X_{Anethole}$ = 0.5 at 45 °C; (14) $X_{Anethole}$ = 0.71 at 45 °C and; (15) $X_{Anethole}$ = 0.83 at 45 °C, Figure S13: The time trace of the Grubbs' 2nd generation catalysed metathesis reaction between 1-hexene (1) and (*E*)-anethole (2) at 15 ºC (top row), 25 ºC (middle row), and 45 ºC (bottom row), the mole fraction of anethole is indicated on each graph. (*E*)-anethole (red -) and 1-hexene (blue -), and the formation of the different products, CM (3, green -), SM 1-hexene (5, purple -) and SM (*E*)-anethole (7, orange -), Figure S14: The time trace of the Grubbs 2nd generation catalysed (*E*)-anethole and 1-hexene (XAnethole ≈ 0.5) reaction at 25 °C in $CDCl_3$ spiked with (A) 0.2 M 1 (experiment 12), (B) 0.2 M 2 (experiment 13) and (C) 0.2 M 1 and 0.2 M 2 at 1086 min (experiment 14), Figure S15: The time traces of the of the initial 20 min of the Grubbs' 2nd generation catalysed metathesis reaction between 1-hexene (1) and (*E*)-anethole (2) at 15 °C (left), 25 °C (middle), and 15 °C (right), the mole fraction of anethole is indicated on each graph, Figure S16: Graph of % distribution of metathesis products 3, 5, and 7 vs. XAnethole at the different temperatures (as indicated) at the time where [3]max was reached, Figure S17: The kinetic plots of the disappearance of 1 (blue) and 2 (yellow) at (left) 25 °C and (right) 45 °C for the metathesis reactions (at the indicated XAnethole) that leads to the apparent observed first order rate constant k'obs, Figure S18: Graph comparing the TOF at the time when [3]max is reached against the reaction conditions.

Author Contributions: Conceptualization, E.E. and C.M.; methodology, M.R.S. and E.E.; validation, E.E. and C.M.; investigation, M.R.S.; resources, E.E. and C.M.; data curation, M.R.S.; writing—original draft preparation, M.R.S.; writing—review and editing, E.E. and C.M.; visualization, M.R.S., C.M. and E.E.; supervision, E.E. and C.M.; funding acquisition, E.E. and C.M. All authors have read and agreed to the published version of the manuscript.

Funding: This research was funded by the South African National Research Foundation, grant numbers 119028 (EE) and 118076 (CM). Additional financial support from Sasol and the Central Research Fund of the University of the Free State, Bloemfontein, South Africa is also acknowledged and greatly appreciated.

Conflicts of Interest: The authors declare no conflict of interest.

References

1. Bruneau, C.; Fischmeister, C.; Miao, X.; Malacea, R.; Dixneuf, P.H. Cross-Metathesis with Acrylonitrile and Applications to Fatty Acid Derivatives. *Eur. J. Lipid Sci. Technol.* **2010**, *112*, 3–9. [CrossRef]
2. Connon, S.J.; Blechert, S. Recent Developments in Olefin Cross-Metathesis. *Angew. Chem. Int. Ed.* **2003**, *42*, 1900–1923. [CrossRef]
3. Morzycki, J.W. Application of Olefin Metathesis in the Synthesis of Steroids. *Steroids* **2011**, *76*, 949–966. [CrossRef]
4. Schuster, M.; Blechert, S. Olefin in Metathesis in Organic Chemistry. *Angew. Chem. Ed. Engl.* **1997**, *36*, 2036–2056. [CrossRef]
5. Herndon, J.W. The Chemistry of the Carbon-Transition Metal Double and Triple Bond: Annual Survey Covering the Year 2018. *Coord. Chem. Rev.* **2019**, *401*, 213051. [CrossRef]
6. Ogba, O.M.; Warner, N.C.; O'Leary, D.J.; Grubbs, R.H. Recent Advances in Ruthenium-Based Olefin Metathesis. *Chem. Soc. Rev.* **2018**, *47*, 4510–4544. [CrossRef] [PubMed]
7. Müller, D.S.; Baslé, O.; Mauduit, M. A Tutorial Review of Stereoretentive Olefin Metathesis Based on Ruthenium Dithiolate Catalysts. *Beilstein J. Org. Chem.* **2018**, *14*, 2999–3010. [CrossRef]
8. Dong, Y.; Matson, J.B.; Edgar, K.J. Olefin Cross-Metathesis in Polymer and Polysaccharide Chemistry: A Review. *Biomacromolecules* **2017**, *18*, 1661−1676. [CrossRef]
9. Thangavel, M.; Chin, S.Y. Cross-Metathesis of Plant Oil: A Mini Review on Reaction Condition and Catalysis. *IOP Conf. Ser. Mater. Sci. Eng.* **2020**, *991*, 012073. [CrossRef]
10. Sinclair, F.; Alkattan, M.; Prunet, J.; Shaver, M.P. Olefin Cross-Metathesis and Ring-Closing Metathesis in Polymer Chemistry. *Polym. Chem.* **2017**, *8*, 3385–3398. [CrossRef]
11. Lin, Y.A.; Chalker, J.M.; Davis, B.G. Olefin Cross-Metathesis on Proteins: Investigation of Allylic Chalcogen Effects and Guiding Principles in Metathesis Partner Selection. *J. Am. Chem. Soc.* **2010**, *132*, 16805–16811. [CrossRef]

12. Ritter, T.; Hejl, A.; Wenzel, A.G.; Funk, R.W.; Grubbs, R.H. A Standard System of Characterization for Olefin Metathesis. *Organometallics* **2006**, *25*, 5740–5745. [CrossRef]
13. Chatterjee, A.K.; Sanders, D.P.; Grubbs, R.H. Synthesis of Symmetrical Trisubstituted Olefins by Cross Metathesis. *Org. Lett.* **2002**, *4*, 1939–1942. [CrossRef]
14. Vummaleti, S.V.C.; Cavallo, L.; Poater, A. The Driving Force Role of Ruthenacyclobutanes. *Theor. Chem. Acc.* **2015**, *134*, 22. [CrossRef]
15. Chatterjee, A.K.; Choi, T.-L.; Sanders, D.P.; Grubbs, R.H. A General Model for Selectivity in Olefin Cross Metathesis. *J. Am. Chem. Soc.* **2003**, *125*, 11360–11370. [CrossRef]
16. Allaert, B.; Ledoux, N.; Dieltiens, N.; Vander Mierde, H.; Stevens, C.V.; Van Der Voort, P.; Verpoort, F. Secondary Metathesis with Grubbs Catalysts in the 1,4-Polybutadiene System. *Catal. Commun.* **2008**, *9*, 1054–1059. [CrossRef]
17. Anderson, D.R.; Ung, T.; Mkrtumyan, G.; Bertrand, G.; Grubbs, R.H.; Schrodi, Y. Kinetic Selectivity of Olefin Metathesis Catalysts Bearing Cyclic (Alkyl)(Amino)Carbenes. *Organometallics* **2008**, *27*, 563–566. [CrossRef]
18. Montgomery, T.P.; Johns, A.M.; Grubbs, R.H. Recent Advancements in Stereoselective Olefin Metathesis Using Ruthenium Catalysts. *Catalysts* **2016**, *6*, 87. [CrossRef]
19. Shahane, S.; Bruneau, C.; Fischmeister, C. *Z* Selectivity: Recent Advances in One of the Current Major Challenges of Olefin Metathesis. *ChemCatChem* **2013**, *5*, 3436–3459. [CrossRef]
20. Gottumukkala, A.L.; Madduri, A.V.R.; Minnaard, A.J. Z-Selectivity: A Novel Facet of Metathesis. *ChemCatChem* **2012**, *4*, 462–467. [CrossRef]
21. Zhu, W.; Gunnoe, T.B. Advances in Rhodium-Catalyzed Oxidative Arene Alkylation. *Acc. Chem. Res.* **2020**, *53*, 920–936. [CrossRef]
22. Webster-Gardiner, M.S.; Chen, J.; Vaughan, B.A.; McKeown, B.A.; Schinski, W.; Gunnoe, T.B. Catalytic Synthesis of "Super" Linear Alkenyl Arenes Using an Easily Prepared Rh(I) Catalyst. *J. Am. Chem. Soc.* **2017**, *139*, 5474–5480. [CrossRef] [PubMed]
23. Vasseur, A.; Bruffaerts, J.; Marek, I. Remote Functionalization Through Alkene Isomerization. *Nature Chem.* **2016**, *8*, 209–219. [CrossRef] [PubMed]
24. Sarkic, A.; Stappen, I. Essential Oils and Their Single Compounds in Cosmetics—A Critical Review. *Cosmetics* **2018**, *5*, 11. [CrossRef]
25. Diep, P.T.M.; Pawlowska, A.M.; Cioni, P.L.; Nghi, D.H.; Huong, L.M.; Minh, C.V.; Braca, A. Chemical and Biological Studies of the Essential Oils of *Micromelum hirsutum*. *Nat. Prod. Commun.* **2007**, *2*, 691–694. [CrossRef]
26. Ilijeva, R.; Buchbauer, G. Biological Properties of Some Volatile Phenylpropanoids. *Nat. Prod. Commun.* **2016**, *11*, 1616–1629. [CrossRef]
27. Carrasco, M.R.; Nikitine, C.; Hamou, M.; de Bellefon, C.; Thieuleux, C.; Meille, V. Self-Metathesis of Methyl Oleate Using Ru-NHC Complexes: A Kinetic Study. *Catalysts* **2020**, *10*, 435. [CrossRef]
28. Samojłowicz, C.; Bieniek, M.; Grela, K. Ruthenium-Based Olefin Metathesis Catalysts Bearing N-Heterocyclic Carbene Ligands. *Chem. Rev.* **2009**, *109*, 3708–3742. [CrossRef]
29. Tsedalu, A.A. A Review on Olefin Metathesis Reactions as a Green Method for the Synthesis of Organic Compounds. *J. Chem.* **2021**, *2021*, 3590613.
30. Van der Gryp, P.; Marx, S.; Vosloo, H.C.M. Experimental, DFT and Kinetic Study of 1-Octene Metathesis with Hoveyda-Grubbs Second Generation Precatalyst. *J. Mol. Catal. A Chem.* **2012**, *355*, 85–95. [CrossRef]
31. Moussaoui, Y.; Saïd, K.; Salem, R.B. Anionic Activation of the Wittig Reaction Using a Solid-Liquid Phase Transfer: Examination of the Medium-, Temperature-, Base- and Phase-Transfer Catalyst Effects. *ARKIVOC* **2006**, *12*, 1–22. [CrossRef]
32. Guerrini, A.; Sacchetti, G.; Muzzoli, M.; Rueda, G.M.; Medici, A.; Besco, E.; Bruni, R. Composition of the Volatile Fraction of *Ocotea bofo* Kunth (Lauraceae) Calyces by GC-MS and NMR Fingerprinting and Its Antimicrobal and Antioxidant Activity. *J. Agric. Food Chem.* **2006**, *54*, 7778–7788. [CrossRef]
33. Hanna, S.; Buthcher, T.W.; Hartwig, J.F. Contra-thermodynamic Olefin Iomerization by Chain-Walking Hydrofunctionalization and Formal Retro-hydrofunctionalization. *Org. Lett.* **2019**, *21*, 7129–7133. [CrossRef]
34. Nelson, D.J.; Manzini, S.; Urbina-Blanco, C.A.; Nolan, S.P. Key Processes in Ruthenium-Catalysed Olefin Metathesis. *Chem. Commun.* **2014**, *50*, 10355–10375. [CrossRef]
35. Grela, K. *Olefin Metathesis Theory and Practice*; Wiley: Hoboken, NJ, USA, 2014; p. 40.
36. Yang, G.; Lee, J.K. Curing Kinetics and Mechanical Properties of endo-Dicyclopentadiene Synthesized Using Different Grubbs' Catalysts. *Ind. Eng. Chem. Res.* **2014**, *53*, 3001–3011. [CrossRef]
37. Thiel, V.; Hendann, M.; Wannowius, K.-J.; Plenio, H. On the Mechanism of the Initiation Reaction in Grubbs–Hoveyda Complexes. *J. Am. Chem. Soc.* **2011**, *134*, 1104–1114. [CrossRef]
38. Sanford, M.S.; Love, J.A.; Grubbs, R.H. Mechanism and Activity of Ruthenium Olefin Metathesis Catalysts. *J. Am. Chem. Soc.* **2001**, *123*, 6543–6554. [CrossRef]
39. Forcina, V.; Garcia-Dominguez, A.; Lloyd-Jones, G.C. Kinetics of Initiation of the Third Generation Grubbs Metathesis Catalyst: Convergent Associative and Dissociative Pathways. *Faraday Discuss.* **2019**, *220*, 179–195. [CrossRef] [PubMed]
40. Hyatt, M.G.; Walsh, D.J.; Lord, R.L.; Andino Martinez, J.G.; Guironnet, D. Mechanistic and Kinetic Studies of the Ring Opening Metathesis Polymerization of Norbornenyl Monomers by a Grubbs Third Generation Catalyst. *J. Am. Chem. Soc.* **2019**, *141*, 17918–17925. [CrossRef]

41. Dinger, M.B.; Mol, J.C. High Turnover Numbers with Ruthenium-Based Metathesis Catalysts. *Adv. Synth. Catal.* **2002**, *344*, 671–677. [CrossRef]